Predictions of Aneurysm Formation in Distensible Tubes
Part B – Application and Comparison of Alternative Approaches

Andrea Bucchi[* (a)] and Grant E. Hearn [(b)]

(a) School of Engineering, University of Portsmouth, United Kingdom

(b) Fluid Structure Interaction Research Group – Faculty of Engineering and the Environment, University of Southampton, United Kingdom

Abstract

The theoretical treatise of the companion paper produced three distinct approaches of increasing complexity. Just as the presented theory is equally applicable to other medical, scientific or engineering applications, so the systematic numerical investigation now reported is relevant to these fields of study. An independently developed finite element analysis (FEA) solution is used to show that the commercial package selected provides critical pressure predictions of a consistent order of magnitude. The FEA sensitivity analysis considers five distinct elements with up to seven alternative strain-energy functions and different combinations of uniaxial, equi-biaxial and pure shear data sets to identify the effect on critical pressure prediction and overall behaviour of a pressurised distensible tube. This represents the most comprehensive comparative study available in the open literature. For a selected strain-energy function the impact of the variation of length to initial radius and wall thickness to initial radius are investigated. Thereafter it is demonstrated that these two ratios rather than actual dimensions are the driving factors behind pressurised tube behaviour.

---

[*] Corresponding author, e-mail address: Andrea.Bucchi@port.ac.uk

1. Introduction

In the previous paper [1] three distinct numerical techniques with differing levels of prediction capability and efficiency were discussed. The limited qualitative results presented, for various strain-energy functions, used the combined uniaxial, equi-biaxial and pure shear stress strain data made available by Treloar [2] and Kawabata et al. [3]. It is rather surprising that no other experimental data set exists in the open literature; where authors have claimed to provide their own data, close examination seems to suggest that the material is not significantly different to that used by Treloar in the 1940s. The semi-analytic, very long thin walled tube approach of Section 3.1 of [1] is useful in providing basic estimates to initiate the more complex membrane analysis outlined in Section 3.2 of [1]. This latter analysis established some confidence in the FEA predictions presented by providing comparable values of critical pressure and 3D tube shapes at different stages of inflation. The FEA sensitivity are then further appreciated through observation of the influence of the element choice made, the strain-energy function selected and the extent of the data sets used.

1.1 Organization of paper

In this paper alternative FEA elements, are considered to further establish confidence in this approach. Within the theoretical companion paper [1], sample FEA was only based on the S4R shell element. In Section 2 different alternative boundary conditions are justified regarding specific applications. In Section 3 reworking of the analysis of Shi & Moita [4] indicates consistency of predictions whether using their particular FEA or the package selected by the authors. Finite element application sensitivity is addressed through variation of the total number of elements and the element distribution utilized, and the impact upon predicted behaviour of the inflated distensible tube. In the in-depth numerical study of Section 4 alternative finite elements are each considered in turn for several strain-energy functions and various combinations of uniaxial, equi-biaxial and pure shear data sets using Treloar [2] and Kawabata et al. [3] experimental measurements. Some of the strain-energy functions applied in medical studies, such as hemodynamic related aneurysm [5] and arterial stenoses [6], and distensible tubes consist of differing body tissues are either quite distinct [5] or similar to those used in engineering [6,7]. In Section 5 variation of behaviour through geometric characteristics such as tube length to initial radius and wall thickness to initial radius is explored. Finally predictions based on the small scale tube (consistent with most of the publications cited in the theoretical paper [1]) are compared. The finite element method is finally applied to a slightly more complex rubber geometry analogous in form and dimension to that of abdominal aorta

and its iliac branches. The results are presented and discussed in Section 6. Key observations provide paper closure in Section 7.

2. Justification of boundary condition selection

The procedure presented in this research is quite general and can be used for different applications. A parametric analysis on the effect of different boundary conditions, on the predicted value of the pressure, is not carried out because when a particular problem is analysed, appropriate boundary conditions should be selected. For example, in [7] the abdominal aorta is constrained in longitudinal displacement at the upper and lower ends of the aorta due to existence of specific important arteries and organs. In contrast fully clamped conditions are deliberately used in the experimental set up of a wave energy device known to experience aneurysm under certain conditions [8]. In references [9, 10] end conditions are not explicitly stated within the context of the finite element analysis undertaken, but within the experiments used to provide comparing measurements it would appear that fully clamped boundary conditions is the most likely description of the experimental set-up. Yet another boundary condition is the clamped-rolled FEA model presented in Figure 10 of [1]. The variation of critical pressure in this case is just 1.93% different to the corresponding clamped-clamped analysis represented in Figure 9 of [1]. Out of curiosity a comparisons of fully clamped and pinned conditions were compared for different strain-energy function and again the difference in critical pressure varied from 0.02% to 1.52%. With this small apparent differences due to changes in boundary conditions and the large matrix of studies to be undertaken through variation of element selection, strain-energy function choice and data sets combination for calibration of two different materials, no further investigation of boundary conditions will be undertaken in this paper and the mesh sensitivity is carried out assuming both tube ends are fully clamped. As consequence of this decision we will demonstrate later that the length of the tube is not affecting the magnitude of the predicted critical pressure.

3. Reworking of Shi & Moita problem

Shi & Moita [4] developed their own finite element solution based on a hyper-elastic material with an axisymmetric membrane element. This permits comparison of two distinct FEA, rather than limited finite element comparison for different elements available in a single commercial package. The length of the tube in [4] is partitioned into an unknown number of elements of two nodes, with the strain-energy function corresponding to an Ogden fitting [11] of all the original Treloar data

using a third-order Ogden model. The numerical values of the parameter pairs $\alpha_i, \mu_i : i = 1, 2 \& 3$ [4, 11] are:

$$\alpha_1 = 1.3, \ \alpha_2 = 5.0, \ \alpha_3 = -2.0 \ \text{and} \ \mu_1 = 6.3 \, kg/cm^2, \ \mu_2 = 0.012 \, kg/cm^2, \ \mu_3 = -0.1 \, kg/cm^2. \quad (1)$$

Tube dimensions correspond to $2l_0/r_0 = 20$ and $t_{w0}/r_0 = 0.1$ for an initial length of $2l_0 = 200$mm, initial mean radius of $r_0 = 10$mm and initial wall thickness $t_{w0} = 1$mm. The predicted critical pressure of Shi & Moita [4] is compared with predictions from a commercial package using the same Ogden parameters for three distinct finite element types. To appreciate sensitivity of analysis to assigned values of parameters $\alpha_i, \mu_i : i = 1, 2 \& 3$, the same three finite elements and the Ogden strain-energy function with least-squares fitted parameters recovered from the Treloar data (Appendix A of [1]) is presented. The three distinct finite elements used together with the tube particulars are provided in Figure 1.
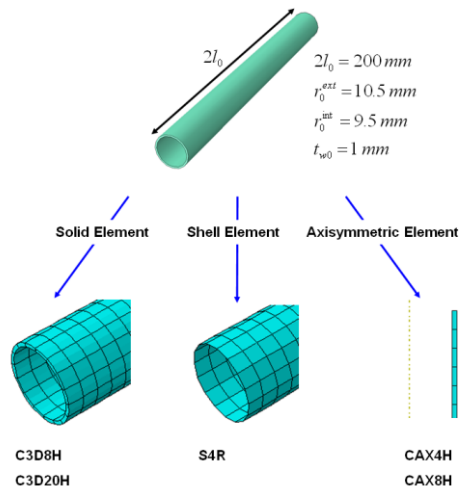

Fig. 1. Different finite element representations of the physical model

Variation of the finite element meshes, adopted by the authors, in their use of the solid and shell elements are presented in Figure 2.
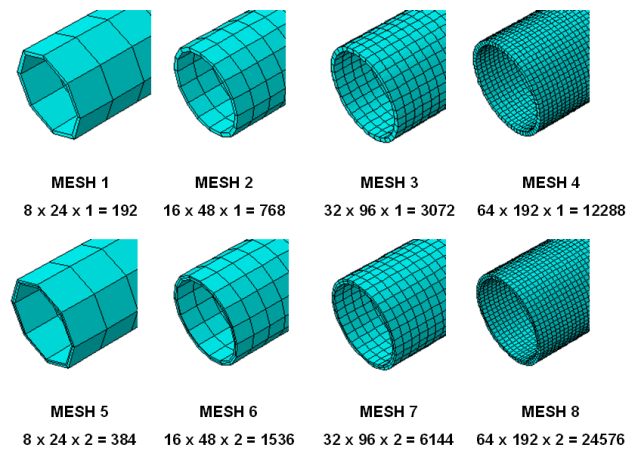

Fig. 2. Different refinement of finite element mesh

4

The meshes of Figure 2 are defined by $N_c \times N_l \times N_t$ representing number of circumferential, longitudinal and through-wall elements respectively. For the simplified axisymmetric element representations (CAX4H, CAX8H) the finite element distribution longitudinally is the same, but no elements are required circumferentially. N_c is still used in the total element count for the simplified axisymmetric elements for comparison purposes. For solid elements and shell elements the geometric aspect ratio is approximately unity.

Each mesh refinement consists of the doubling of the number of elements longitudinally and circumferentially. Meshes 1 and 2 are deliberately small to determine whether their associated predictions are radically different to the more extensive meshes. Mesh 3 is considered adequate since this discretization uses approximately twice the elements used in [9, 10] and is comparable with [7]. Mesh 4 represents a more extreme level of discretization. Meshes 5 to 8 are reserved for the solid element, since in this case wall thickness is modelled using two elements. For solid or axisymmetric elements the initial internal and external radius is $r_0^{\text{int}} = 9.5$mm and $r_0^{ext} = 10.5$mm. For a shell element the mean initial radius of $r_0 = 10$mm represents the middle plane.

3.1 Mesh sensitivity

A three-term Ogden [11] model is used to describe material behaviour. Shi & Moita [4] provide no tabulated values of critical pressure and so numerical values are recovered from their plot of P^*/μ. The critical pressure P_{cr}^* corresponds to $P^*/\mu = 0.08$. Using values of (α_i, μ_i) defined in column 3 of Table 1, the value of $\mu = 4.225 kg/cm^2$ is obtained using $\mu = \frac{1}{2}\sum_{i=1}^{3} \alpha_i \mu_i$ and

hence $P_{cr}^* = 3.32 \cdot 10^4 Pa$. Since the actual number of axisymmetric membrane elements used by Shi & Moita [4] is not specified the estimated P_{cr}^* is treated as invariant with the number of elements. The sensitivity analysis will be presented in two parts. Initially the influence of each selected ABAQUS[®] element for each Figure 2 mesh is compared with the estimated Shi & Moita based prediction of critical pressure. In the second case the influence of using slightly different Ogden parameters is demonstrated using the ABAQUS[®] software to fit the Treloar data (Appendix A of [1]) and Ogden's fitting of Treloar data [11]. Table 1 sets out the corresponding Ogden's parameter derived from the ABAQUS[®] fitting of Appendix A [1] data using Equations (15) and (16) of [1] together with the Shi & Moita values.

Table 1 Variation in Ogden strain-energy function parameters

ABAQUS® fitting of Appendix A [1] based on Equation (16) of [1]	ABAQUS® fitting of Appendix A [1] based on Equation (15) of [1]	Original values used by Shi & Moita [4] consistent with Equation (15) of [1]
$\mu_1 = 398206.801$ Pa	$\mu_1 = 7.173\,kg/cm^2$	$\mu_1 = 6.3\,kg/cm^2$
$\mu_2 = 5377.71517$ Pa	$\mu_2 = 0.023\,kg/cm^2$	$\mu_2 = 0.012\,kg/cm^2$
$\mu_3 = 7647.41545$ Pa	$\mu_3 = -0.073\,kg/cm^2$	$\mu_3 = -0.1\,kg/cm^2$
$\alpha_1 = 1.13176086$	$\alpha_1 = 1.13176086$	$\alpha_1 = 1.3$
$\alpha_2 = 4.73211925$	$\alpha_2 = 4.73211925$	$\alpha_2 = 5.0$
$\alpha_3 = -2.14619240$	$\alpha_3 = -2.14619240$	$\alpha_3 = -2.0$

Figures 3a & b illustrate how critical pressure varies with each finite element selected and total number of elements utilized. In Figure 3a the Ogden fitted parameter values are those used by Shi & Moita, whereas in the Figure 3b the parameter values correspond to the second column of Table 1. Figure 3b clearly indicates the influence of different fitting of the Ogden model to the Treloar data.

In the companion paper [1], and in subsequent studies reported in this paper, we have not used the third-order Ogden fitted parameters [11], column 3 of Table 1, since this could adversely affect the comparison predictions based on alternative strain-energy functions. The differences between Figures 3a & b clearly reflect the influence of different researchers fitting of the Treloar data. When exactly the same material parameters are forced into the finite element analysis (Figure 3a) the comparison with Shi & Moita is very consistent despite not having details of Shi & Moita mesh distribution.
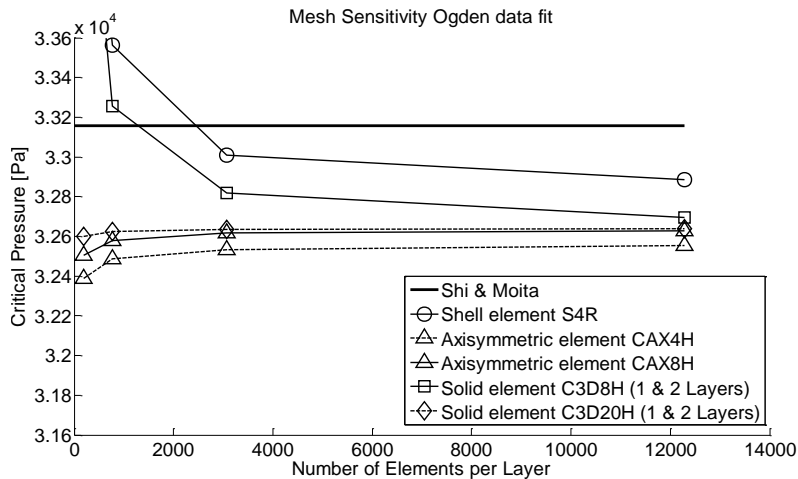

Fig. 3a. Mesh sensitivity with different elements for Ogden [11] Treloar-data fit
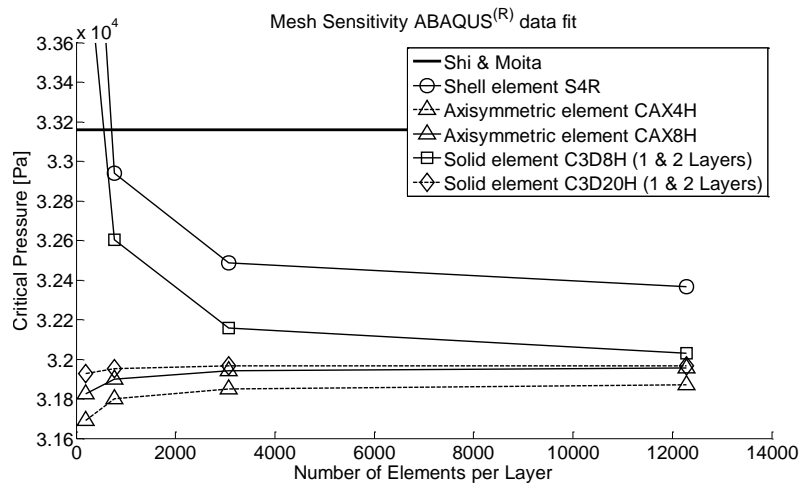
Fig. 3b. Mesh sensitivity with different elements for ABAQUS® Treloar-data fit based on Appendix A [1]

The ABAQUS® elements selected in the comparisons of Figure 3 are not membrane elements, so it is worthwhile recalling that the solid elements (axisymmetric or 3D) are the most general and involve no fundamental assumptions regarding solution of the elastic problem formulation. The shell element takes advantage of the thinness of the structure. Hence a representative middle plane bounded by the faces of the structure is used as if it were the material surface. The shell element selected may adopt thin or thick shell theory; the difference being maintenance or relaxation of shear deformation. When all the moment expressions of a shell formulation are disregarded, the resulting element degenerates to that of a membrane element. Having summarised these differences one may readily deduce from Figure 3 that: meshes 3 & 4 do not lead to substantial differences; two layers model provide no improvement; as the sophistication of the element chosen increases the difference between selected element and Shi & Moita membrane. However, the maximum difference (rejecting meshes 1 & 2, as might be anticipated) does not exceed 1.88% (relative to Shi & Moita value) on inspection of the ordinate of Figure 3 or the numerical values of Table 2 providing critical pressure for the two cited alternative fittings of the Treloar data, using mesh 3.

Table 2 Sensitivity of critical pressure with element variation and Treloar-data fit adopted.

Element (Mesh 3)	Ogden data fit & (Relative Error)	ABAQUS® data fit & (Relative Error)
Shell element S4R	33010.0Pa（−0.45%）	32487.7Pa（−2.02%）
Solid element C3D8H (1 layer)	32819.1Pa（−1.02%）	32157.9Pa（−3.02%）
Solid element C3D8H (2 layers)	32821.7Pa（−1.01%）	32160.6Pa（−3.01%）
Solid element C3D20H (1 layer)	32636.0Pa（−1.57%）	31964.8Pa（−3.60%）
Solid element C3D20H (2 layers)	32645.7Pa（−1.54%）	31975.7Pa（−3.57%）
Axisymmetric element CAX4H	32533.1Pa（−1.88%）	31848.6Pa（−3.95%）
Axisymmetric element CAX8H	32616.0Pa（−1.63%）	31942.1Pa（−3.67%）

Therefore one may conclude that giving the same geometry and the same material properties, the physical problem is consistently modelled by each selected element by authors or Shi & Moita. Furthermore, there is no need for mesh 4 or adoption of 2 layers through the wall thickness. This comparison of ABAQUS® based predictions with an independent finite element suite and the following comparison with a semi-analytic method provides objective confidence (rather than blind faith) in the use of the selected suite.

Reverting to Figures 3a & b we observe the following regarding the specific behaviour of each chosen element:

- Geometrically the reduced integration shell element S4R and the Shi & Moita axisymmetric membrane element are very similar in terms of structure idealization, using the middle plane or line respectively to represent the whole structure. This is probably why prediction differences are minimal.

- Convergence of the linear solid hybrid element (C3D8H) is significantly slower than that of the quadratic solid hybrid element (C3D20H), which is almost instantaneous. The predicted critical pressures for meshes 1 and 2 are sufficiently different to be rejected. Meshes 3 and 4 provide more consistent values.

- The axisymmetric element based predictions are relatively insensitive to the total number of elements used. The difference between linear (CAX4H) and quadratic (CAX8H) hybrid axisymmetric elements is small (less than 0.3%) compared with the behaviour of corresponding solid elements.

- The quadratic solid element (C3D20H), which is the most demanding in computer processor time, provides essentially the same prediction as the less demanding quadratic axisymmetric element (CAX8H) for each mesh.

Comparison with the Shi & Moita study indicates that the quadratic solid element (C3D20H), the linear shell element (S4R) and the quadratic axisymmetric element (CAX8H) are sufficient to represent the finite element technique.

4. A generalized comparative study of critical pressure predictions

Earlier representative pressure predictions against radial stretch [1] and the comparative studies of the previous section have used all three distinct sets of experimental data to determine the parameters of the selected strain-energy function. In this general comparative study the following choices will be collectively explored:

- Influence of Treloar [2] and Kawabata et al. [3] rubber materials.
- Seven distinct combinations of data for a selected material; three individual data sets (where meaningful), three different pairings and one complete data sets.
- Sensitivity to selected strain-energy functions (and variants where meaningful) using parameters fits reported in Appendix A.
- Variation of pressure predictions with three alternative analysis methods; in the case of the finite element approach three different elements (S4R, C3D20H & CAX8H) are investigated.

The tube geometry will initially remain unchanged from that used in Section 2 and illustrated in Figure 1. Data fitting for the parameters of each strain-energy function will be undertaken using ABAQUS® software. The initial product of this comparative study is two sets of tabulated data indicating variation of critical pressure with each strain-energy function for each of the 7 possible combinations of data using: (i) the simple long thin-walled tube analysis, (ii) the axisymmetric membrane theory and (iii) the finite element method for each of the three selected element types.

4.1 Comparison of different approaches

Tables B1(a) to (f) and B2(a) to (f) utilizes the Treloar and Kawabata et al. data respectively. These tables are presented in Appendix B so that the flow of discussion is not adversely affected within the main text. Some combinations of material selected and strain-energy functions can lead to a failure to predict critical pressure. Each possibility is addressed next.

Within each table the phrase 'not possible' is inserted when pure shear data alone is utilised with the Mooney-Rivlin and Ogden strain-energy functions. For pure shear $\lambda_3 = 1$, $\lambda_1 = \lambda$ and so $\lambda_2 = 1/\lambda$. Hence $I_1 = I_2$ and the dependence of Mooney-Rivlin (explicitly) and Ogden (implicitly) upon I_1 and I_2 cannot be resolved. The phrase 'not-possible' associated with the Marlow model indicates that this approach does not permit combining distinct experimental data sets. Depending upon the material selected and the strain-energy function used the phrase 'unstable' indicates that the curve fitting procedure, within the ABAQUS® finite element software, declares the material to be unstable over the specified range of strain. Whilst Figures 2 & 3 of companion paper [1] indicate that the range of strain is much larger for the Treloar data, it is the Treloar data that is deemed 'unstable' more often than the much smoother stress-strain curves of the Kawabata et al. data.

Finally the phrase 'no max.' indicates that critical pressure is not explicitly identifiable since the pressure is monotonically increasing.

Inspection of parts (a) to (f) of Appendix B tables, irrespective of material selected, allows direct comparison of:
- Critical pressure for the three specific methods of analysis.
  Direct comparison of parts (a), (b) & (c) or parts (a), (b), & (d) or parts (a),(b) & (e) permit comparison of selecting a particular finite element with the other semi-analytic approaches.
- Consistency, or otherwise, of the finite element approach per se is achieved directly by comparing parts (c), (d) & (e).
- For the shell S4R element comparison of parts (c) and (f) demonstrate that the exploitation of geometric symmetry, to reduce computational effort, does not reduce prediction accuracy.
- Inspection of any single row, within any part of the table, permits understanding of the impact of using different combinations of experimental data for a selected strain-energy

function. A complementary study is to select any column of any table to appreciate the influence (and applicability) of a strain-energy function with selected sets of material data.

- Finally comparing Tables B1 & B2 in any of the above respects permits assessment of the rubber material selected.

4.2 Comparison of different finite elements

In the companion paper [1] it was observed that only the Yeoh and the third-order Ogden strain-energy function yielded a pressure versus λ_1 curve that permitted determination of propagation pressure according to the Maxwell equal area rule. In view of the generality of the Ogden model, and its utilization for rubber [4, 12 -18] and medical applications [6, 19, 20, 21], the third-order Ogden model is now investigated to highlight the following comparisons:

- Pressure variation with radial stretch parameter for the three selected finite elements using the complete Treloar and Kawabata data sets.
- The shell element will be reworked exploiting geometric symmetry to demonstrate that this slightly faster analysis can produce consistent results irrespective of data sets selected.
- For each complete data set pressure variation with radial stretch parameter is reported for the three particular strain-energy functions that capture the maximum likely extent of pressure variation.
- Maximum variation of critical pressure is then presented for each strain-energy function previously defined [1] for each of the three finite elements selected and for all the seven possible combinations of both the Treloar and Kawabata et al. data sets.

Graphical results for each specific comparison purpose are presented next. For reasons stated earlier mesh 3 is used in all subsequent finite element analyses.

4.2.1 Presentation of results

Comparison of parts (c), (d) & (e) of Tables B1 & B2 demonstrates that the choice of finite element in the discretisation process is not particularly significant in terms of critical pressure predictions. This tendency is confirmed for each strain energy function and each of the seven possible combinations of experimental data sets.

The most and least computationally expensive elements are the solid and axisymmetric elements. These elements exhibit excellent agreement in terms of critical pressure and pressure variations

with λ_1. The maximum critical pressure difference of 1.59kPa, using these two elements, occurs when using the Marlow strain-energy function with the uniaxial Treloar data (see Table B1(d) & (e)). The largest discrepancy recorded for all analyses is 1.73kPa. This is associated with the shell and solid elements using a Marlow strain-energy function with Treloar uniaxial data (see Table B1(d) & (f)).

The axisymmetric element, solid and shell element, have slightly different theoretical assumptions [22] and yet provide consistent predictions for the same physical problem, as illustrated in Figures 4a & b.
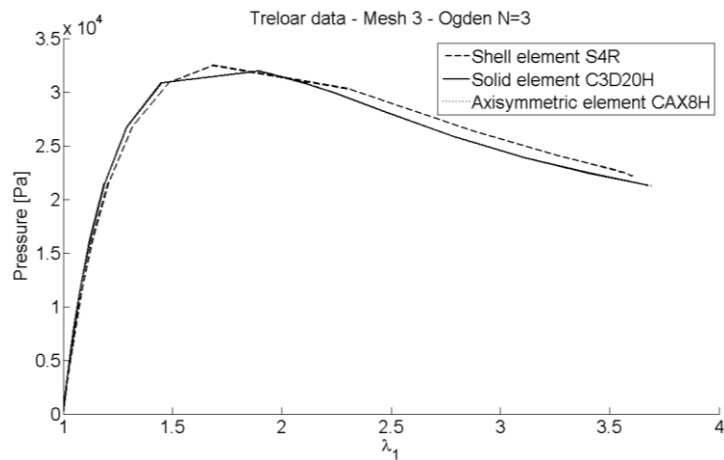
**Fig. 4a. Variation of pressure for different elements using complete set of Treloar experimental data.**
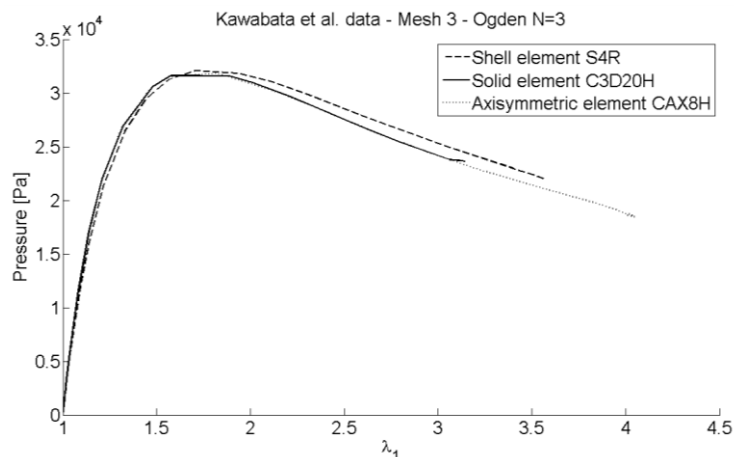

Fig. 4b. Variation of pressure for different elements using complete set of Kawabata et al. experimental data.

Given the similarity of Figure 4a & b, Figure 5 illustrates the evolution of the aneurysm shape as radial stretch is increased for the Treloar material only. The evolution of the aneurysm, for the three

different elements, is captured at two different steps in the solution of the nonlinear elastic equilibrium path with the use of the Riks algorithm [23].
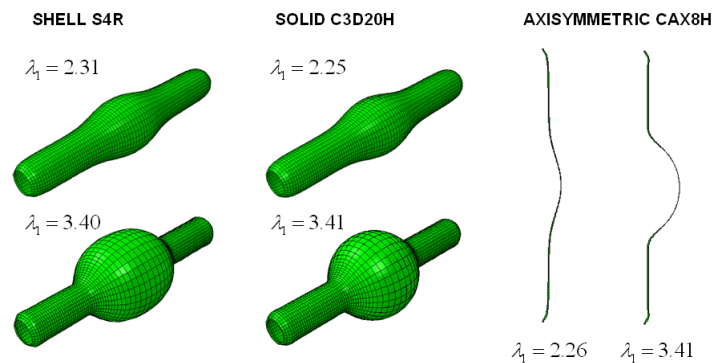
Fig. 5.   Evolution of aneurysm shape using mesh 3 with different finite elements

Figure 5 demonstrates that variation of geometry is self consistent irrespective of element type selected.

4.2.2 Exploitation of geometric symmetry

Most numerical procedures exploit geometric symmetry to reduce mesh size and hence computational effort. For the shell element (only) symmetry across the central x–y plane corresponds to $u_z = 0$ & $\theta_x = \theta_y = 0$. Figures 6a & b provide pressure variation against radial stretch for the equivalent clamped-clamped and the clamped-symmetry boundary condition specified. The clamped-clamped pressure variations of Figures 6a & b are identical with the shell element pressure plots of Figure 4a & b.
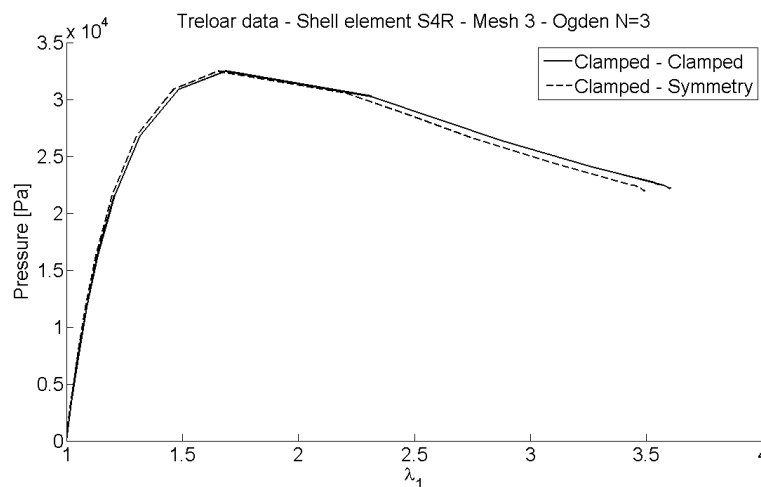
Fig. 6a.   Variation of pressure for different boundary conditions using shell element with complete set of Treloar experimental data.
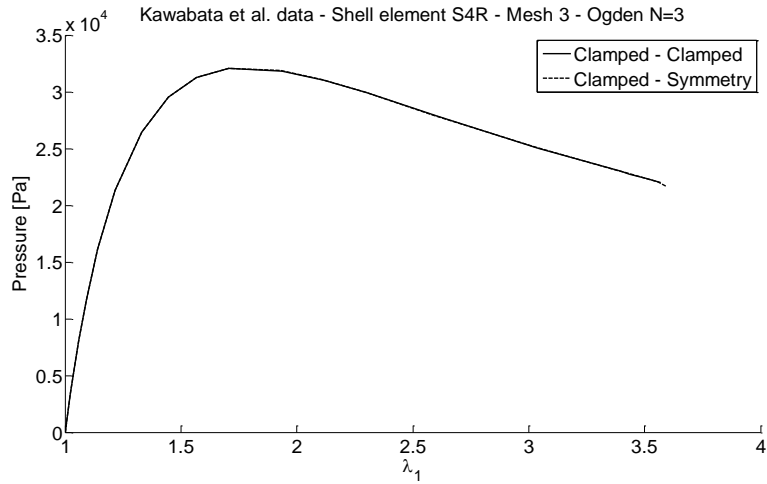
Fig. 6b. Variation of pressure for different boundary conditions using shell element with complete set of Kawabata et al. experimental data.

Figure 6 demonstrates that alternative boundary conditions have no particular effect on the predicted critical pressure. Numerically the proposed symmetry boundary conditions leads to a maximum difference of 0.26kPa when using combined uniaxial and pure shear data with the Yeoh model for the Kawabata et al. material; compare part (c) and (f) of Table B2. Figure 6c provides comparative 3D shapes of the distensible tube for approximately[1] corresponding λ_1-values.
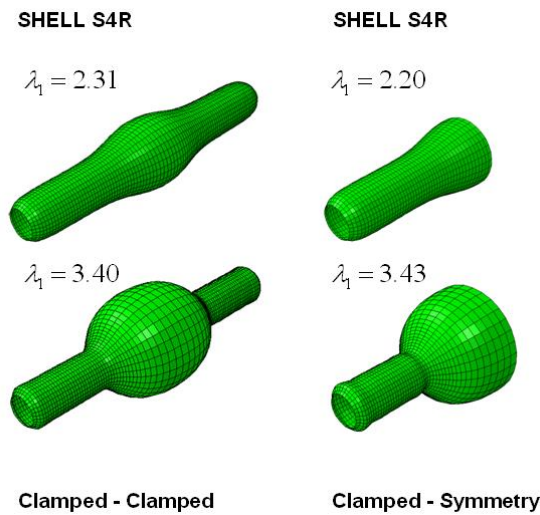
Fig. 6c. Evolution of aneurysm shape using mesh 3, shell element with different BC

---

[1] Variation of λ_1-values within the finite element procedure is automatic. Hence for a reworked analysis using a different element or boundary condition the same sequence of λ_1-values is not repeated.

4.3 Comparison of different strain-energy functions

The motivation to examine the impact of the selected strain-energy function upon predicted critical pressure is their role in the simulation of rubber behaviour using the finite element analysis. In general, within the scientific literature, too often only one strain-energy function is used [4, 9, 10, 12, 15, 16]. Even if two or more strain-energy functions are utilized tabulated numerical values are rarely provided, despite their significant benefit when comparing alternative analyses. The different strain-energy functions explored, defined in the companion paper [1], are generally available within commercial finite element codes. However, the authors have failed to locate any research paper in which several distinct strain-energy functions are utilized with alternative combinations of stress-strain data sets. Figures 7a & b clearly illustrate sensitivity of critical pressure to strain-energy function selected for all possible data set combinations for Treloar and Kawabata et al. materials.
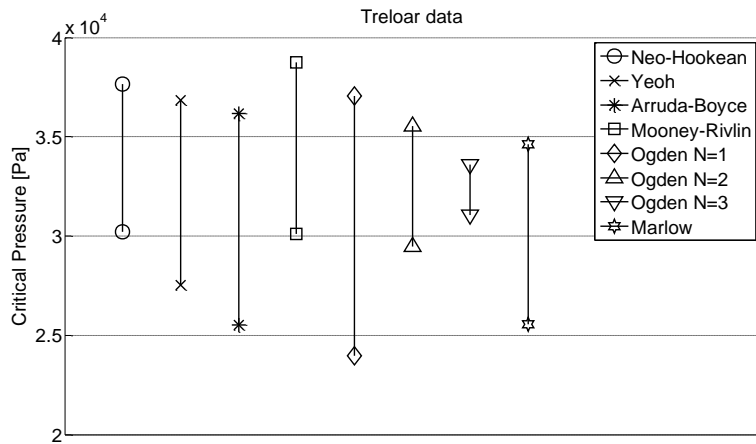
**Fig. 7a.** **Value of critical pressure for alternative finite elements and constitutive rubber-model using Treloar data**
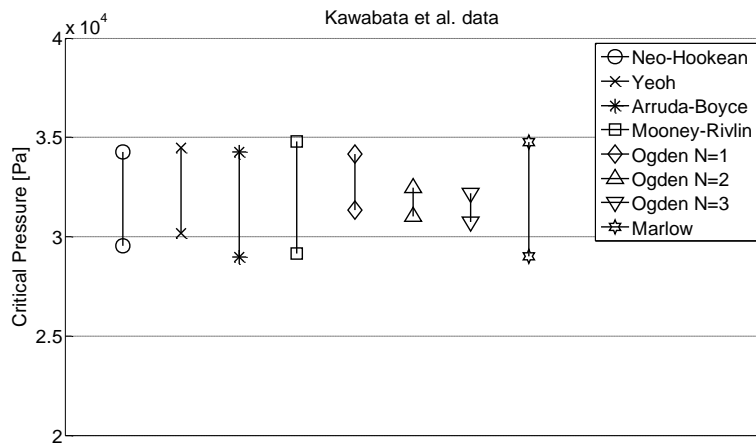

Fig. 7b. **Value of critical pressure for alternative finite elements and constitutive rubber-model using Kawabata et al. data**

The maximum value of 38752.9Pa and minimum value of 23951.7Pa achieved within the Treloar data (Figure 7a) are readily identified in Tables B1(c) & (e). The maximum value is associated with a shell element utilizing the Mooney-Rivlin strain-energy function with the combined uniaxial and equi-biaxial data sets. The minimum value is related to the axisymmetric element using a first-order Ogden model based on uniaxial data.

For the Kawabata data the difference between maximum and minimum values is significantly smaller. The maximum and minimum critical pressure values are 34798.6Pa (Table B2 (c)) and 28988.7Pa (Table B2 (e)). The maximum value is now associated with the shell element using the Mooney-Rivlin strain energy function with equi-biaxial data. The minimum value is for the axisymmetric element using the Arruda-Boyce strain-energy function with uniaxial data.

Other key observations are:
- For both materials the smallest range of critical pressure values are those associated with the second-order and third-order Ogden models.
- The range of predicted critical pressure associated with the Arruda-Boyce and Marlow strain-energy functions are comparable for both materials.
  Hence it would appear that the use of different data set combinations with a reasonably complex Arruda-Boyce strain energy function is no better than the Marlow strain-energy function restricted to a single data set.
- From Tables B1 (c), (d) & (e) we note that using equi-biaxial data only, irrespective of element choice considered, the predicted critical pressure is maximal for Neo-Hookean, Yeoh, Arruda-Boyce, first and second order Ogden models. For these four strain-energy functions the range of critical pressure values is greatest when using uniaxial data only, although the variation due to element choice is negligible.
- Irrespective of the method of analysis employed the minimum critical pressure is always associated with use of uniaxial data alone, whereas the maximum critical pressure is always associated with the use of equi-biaxial data.

These observations demonstrate how finite element predictions can be severely affected through the selection of a strain-energy function. This variability of predictions is due to the fact that some of the strain-energy functions are not capturing the essential behaviour of the physics of material deformation or the intrinsic characteristic of the material [1]. Furthermore, good comparison between numerical/theoretical and experimental results may be achieved as a consequence of an

arbitrary selection of the strain-energy function. Establishing the validity of this choice is often difficult because very often only the fitting parameters of the strain-energy function are reported without any indication of the actual experimental data used [15, 16, 17, 18].

Irrespective of the finite element selected the tabulated numerical values of critical pressure tends to suggest that the strain-energy functions of Arruda-Boyce, Mooney-Rivlin and third-order Ogden models captures the likely range of inflation pressure. This is readily demonstrated in Figures 8a & b, for pressure variation versus radial stretch. This observation is true for both materials selected.
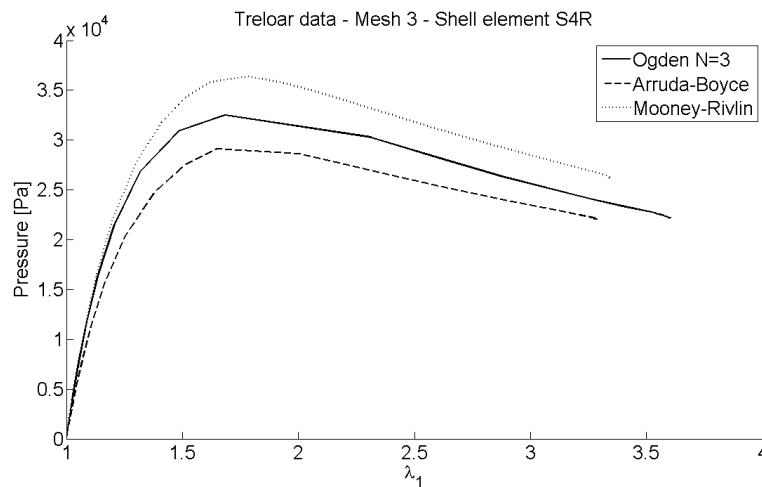
Fig. 8a.   Variation of pressure for shell element (S4R) using different constitutive rubber models with a complete set of experimental Treloar data.
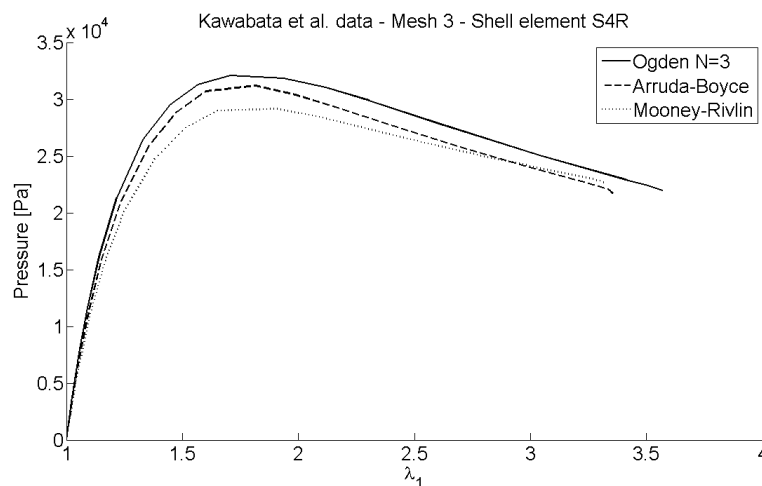
Fig. 8b.   Variation of pressure for shell element (S4R) using different constitutive rubber models with a complete set of experimental Kawabata et al. data.

Figure 7 indicated that the Ogden models have reduced sensitivity to data sets used as the order of models is increased. Since third-order Ogden and Yeoh models consistently satisfy the Maxwell equal area condition for aneurysm propagation, and the variance of the Yeoh model is greater than the third-order Ogden model, Yeoh sensitivity to data set selection is presented in Figures 9a & b using the S4R shell element.

This exploration of the influence of different experimental data sets is a novel occurrence in distensible tube research.

The uniaxial tension test is the most commonly used method [9, 10] to acquire material behaviour information, although this test has been replaced by equi-biaxial test [12], as used by Guo [17], or by uniaxial and pure shear data [15]. Ideally a complete set of experimental data (uniaxial, equi-biaxial and pure shear) should be used to capture the intrinsic behaviour of the material. Figures 9 clearly indicate that pressure distribution is significantly affected by data set(s) selected to identify the Yeoh strain-energy parameters.
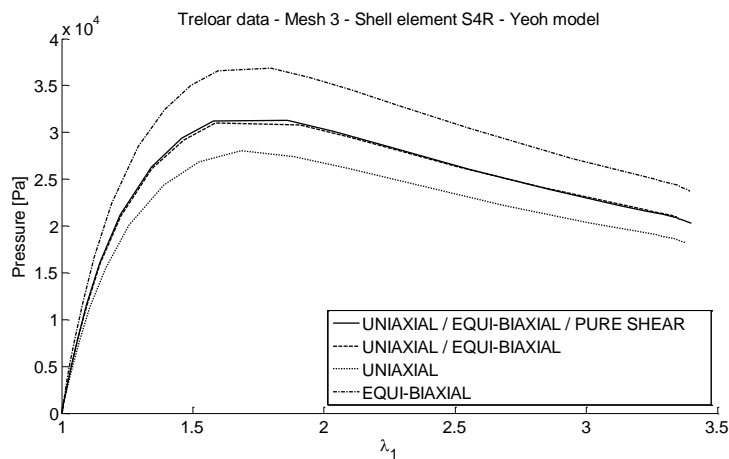
Fig. 9a. Variation of pressure using S4R element and Yeoh model with different combinations of experimental Treloar data
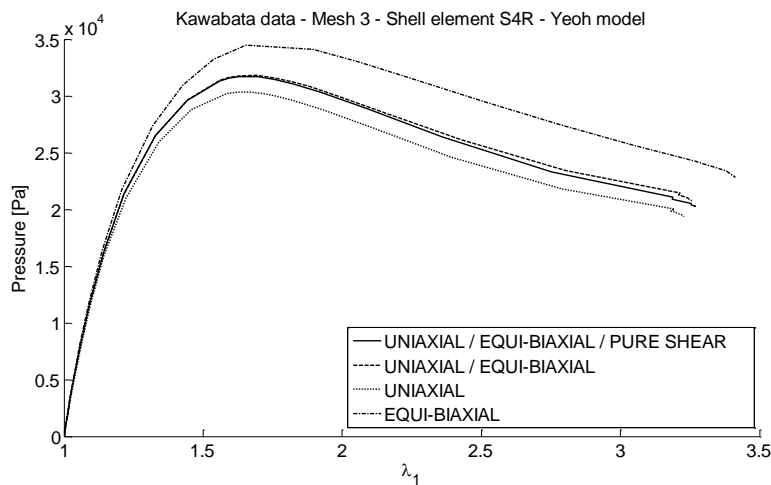
Fig. 9b. Variation of pressure using S4R element and Yeoh model with different combinations of experimental Kawabata et al. data

Numerical results presented confirm that combined uniaxial and equi-biaxial experimental data is suitable for critical pressure prediction.

5. Scaling the model for engineering applications

The distensible tube analysis undertaken previously for fixed values of $2l_0/r_0 = 20$ and $t_{w0}/r_0 = 0.1$ is more appropriate to scientific or medical investigations, see Table 3.

Table 3 Medical distensible tubes dimensions based on [Table B6.1 of 24]

Vessel	Diameter [mm]	Wall thickness [mm]	Length [mm]
Ascending aorta	32	1.6	50–55
Arch of aorta	25–30		40-50
Thoracic aorta	20	1.2	160
Abdominal aorta	17–20	0.9	150
Femoral artery	8	0.5	320
Carotid artery	9	0.75	180
Radial artery	4	0.35	230
Large artery	2–6		
Capillaries	0.005–0.01		
Large veins	5–10		
Vena cava	20		

To widen the scope of the study critical pressure is next investigated for a tube of engineering proportions, mainly:

- For a fixed radius of $r_0 = 10$mm the ratio $2l_0/r_0$ is varied between 10 and 60, whilst the ratio t_{w0}/r_0 lies within the range 0.02 to 0.1.

- For length fixed at $2l_0 = 600$mm the ratio $2l_0/r_0$ is varied between 10 to 60, whilst t_{w0}/r_0 varies within the range 0.02 to 0.1.

Initially $2l_0 \in [100, 600]mm$ and $t_{w0} \in [0.2, 1]mm$ and in the second case $r_0 \in [10, 60]mm$ and $t_{w0} \in [0.2, 6]mm$. These two approaches are essentially equivalent and should generate the same predictions of critical pressure.

Continuing with the shell element, the complete sets of Treloar data and the third-order Ogden model yields the tabulated critical pressures of Tables 4 and 5 respectively.

19

Table 4 Fixed radius FEM critical pressure (Pa) for shell element (S4R) with clamped-symmetry boundary condition, complete Treloar data and third-order Ogden model

	$2l_0/r_0 = 10$	$2l_0/r_0 = 20$	$2l_0/r_0 = 30$	$2l_0/r_0 = 40$	$2l_0/r_0 = 50$	$2l_0/r_0 = 60$
$t_{w0}/r_0 = 0.02$	6577.7	6474.6	6509.8	6515.9	6518.2	not conv.
$t_{w0}/r_0 = 0.04$	13047.6	12968.7	13021.6	13027.6	13044.0	13054.8
$t_{w0}/r_0 = 0.06$	19757.3	19480.1	19536.5	19546.6	19571.0	19552.1
$t_{w0}/r_0 = 0.08$	26351.2	26038.4	26053.6	26076.9	26091.9	26111.0
$t_{w0}/r_0 = 0.10$	32905.4	32485.4	32561.1	32571.5	32585.8	32609.5

Table 4 is easier to read because the radius is fixed. Critical pressure is constant for different values of tube aspect ratio $2l_0/r_0$, in each row of Table 4. That is, critical pressure is insensitive to the tube length. This result is consistent with Shi & Moita [4]. Column variation of critical pressure is almost linear with variation of thickness. This result is in agreement with [10].

Table 5 Fixed length FEM critical pressure (Pa) for shell element (S4R) with clamped-symmetry boundary condition, complete Treloar data and third-order Ogden model

	$2l_0/r_0 = 10$	$2l_0/r_0 = 20$	$2l_0/r_0 = 30$	$2l_0/r_0 = 40$	$2l_0/r_0 = 50$	$2l_0/r_0 = 60$
$t_{w0}/r_0 = 0.02$	6574.6	6471.3	6509.8	6516.1	6518.2	6526.0
$t_{w0}/r_0 = 0.04$	13157.8	12982.7	13021.3	13030.4	13030.7	13054.7
$t_{w0}/r_0 = 0.06$	19749.4	19506.7	19536.3	19546.4	19552.4	19552.0
$t_{w0}/r_0 = 0.08$	26341.0	26036.3	26053.2	26076.7	26091.9	26110.8
$t_{w0}/r_0 = 0.10$	32885.3	32477.3	32571.5	32591.1	32583.2	32637.9

In Table 5 the length is fixed, and the numerical values reported are almost the same as those of Table 4. Essentially in each row the radius is decreasing from left to right, meanwhile wall thickness is increasing down the columns. In a given column the ratio for any two critical pressure values is almost equal to the corresponding ratio of the t_{w0}/r_0 values. That is, for any length, if the thickness is doubled the critical pressure is also doubled, due to higher tube stiffness. The graphical representation of Table 5 is Figure 10.
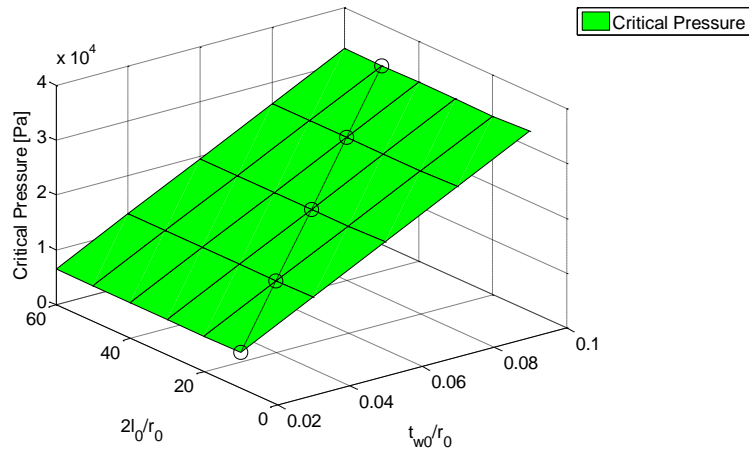
Fig. 10 Critical pressure plane defined by Table 5

The circled values in Figure 10 represent the underlined values in Table 5, which correspond to variation in radius for indicated fixed tube length of 600mm and wall thickness of 1.2mm. Explicit variation of critical pressure with radius is provided in Figure 11, which shows that higher radius values correspond to lower critical pressure values due to t_{w0}/r_0 decreasing, and hence tube stiffness is reducing.
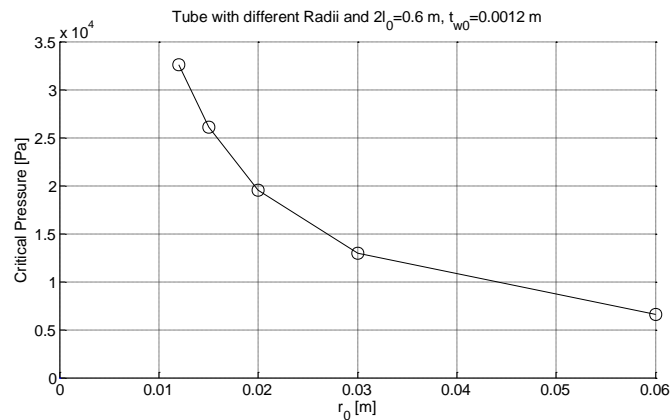
Fig. 11 Influence of tube radius on critical pressure for fixed length and wall thickness

The highlighted values in Tables 4 & 5 indicate the post-buckling shape corresponds to two decentred bulges as illustrated in Figure 12, and not a single centrally located bulge. Clearly the ratio t_{w0}/r_0 is the principal factor influencing aneurysm formation, whilst the ratio $2l_0/r_0$ assumes importance in total rubber costs in engineering applications. The ratio $2l_0/r_0$ cannot avoid aneurysm formation once t_{w0}/r_0 is selected.

21
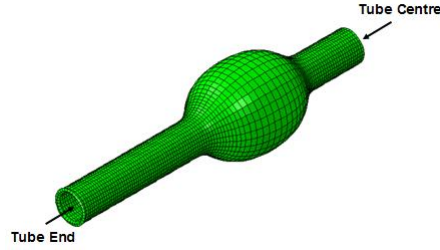
Fig. 12. **One of the two decentred bulges for a half tube**

Variation of pressure versus radial stretch is plotted in Figure 13a for each $2l_0/r_0$ value of Table 4 with $t_{w0}/r_0 = 0.10$. The three dimensional form of the pressurized distensible tube is illustrated in Figure 13b for different values of $2l_0/r_0$, for values of λ_1 closest to 3.15, (see footnote 2). Extension of the aneurysm compared with the overall tube length is clearly controlled by $2l_0/r_0$.
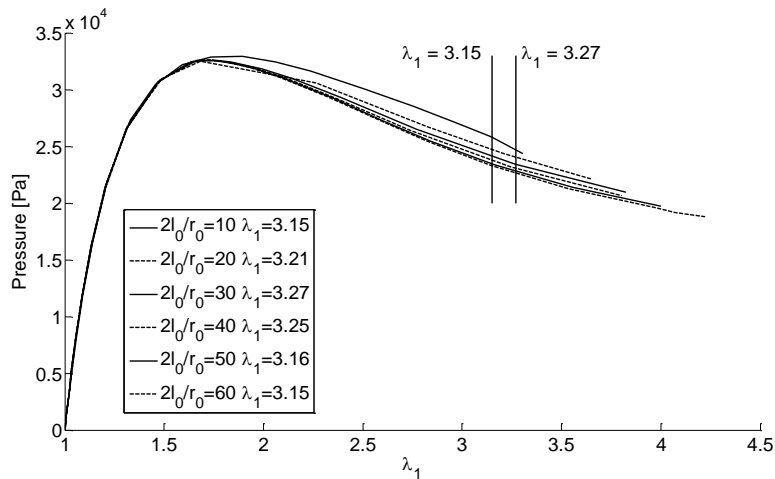
Fig. 13a. **Inflation pressure versus radial stretch for different $2l_0/r_0$ ratios**
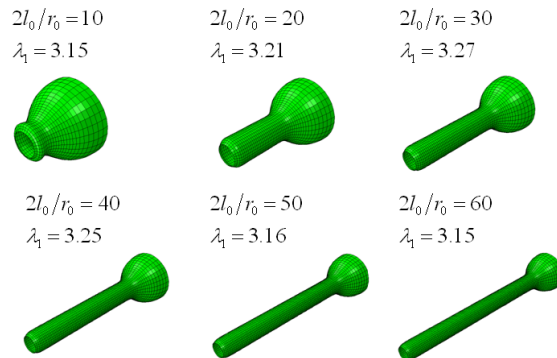
Fig. 13b. **Representation of the aneurysm for different $2l_0/r_0$ ratios**

Having considered a single tube we next consider a branched tube. The relative dimension of the principal tube and branched tubes are consistent with the abdominal aorta and its iliac branches. In engineering, larger scaled branched tubes have been considered to form part of the power take off unit of a wave energy extraction device. Here we consider application of FEA to assessment of critical pressure in a distensible tube, with a geometry analogous to the corresponding abdominal aorta and iliac branches.

6. Analysis of branched tube

The finite element model discussed in the previous sections was of relevance to an existing realistic engineering geometry. The new selected geometry is representative of the abdominal aorta and its iliac branches. Geometric and dimensional details are presented in Figure 14a.
Throughout the wall thickness is considered constant and equal to 0.002m. This value is consistent with data available in the literature [21]. The material properties selected do not reflect human tissue, but the earlier used Treloar rubber presented as uniaxial, equi-biaxial and pure shear data. Hence, the material does not represent the properties of a blood vessel, but is consistent with previous single tube analysis performed.
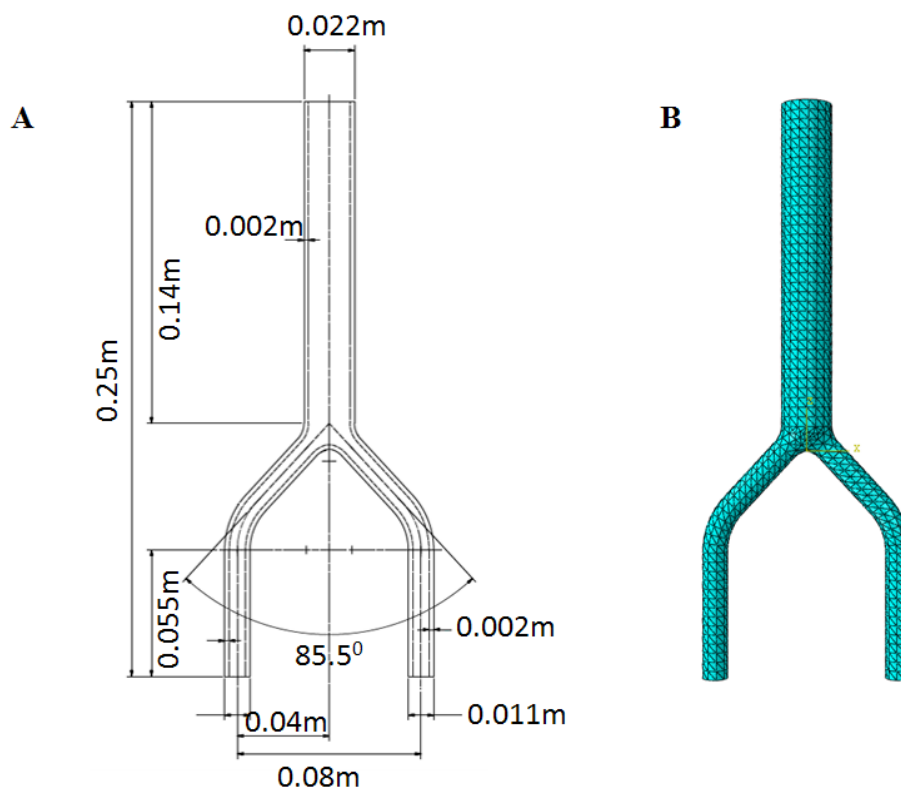
Fig. 14. Geometric dimensions of branched distensible tube used in finite element model [25]

For the finite element simulation a discretization is realized using the quadratic tetrahedral solid element (C3D10H), as illustrated in Figure 14b, with a mixed formulation. The tetrahedral element is analogous to the hexahedral element C3D20H used in previous analyses. The tetrahedral element is preferred in this case to permit an easier automatic mesh generation. The controlling parameter influencing number of tetrahedral elements generated is the maximum allowable tetrahedral edge length presented in Table 6; clearly tetrahedral height does not exceed the wall thickness. As boundary conditions all tube ends are treated as fully clamped. This choice is in agreement with medical investigations [21].

Table 6 Mesh sensitivity

Number of C3D10H elements	Tetrahedral control length	Critical pressure
4764	0.0080m	68963.4Pa
5686	0.0055m	62716.4Pa
7553	0.0040m	62585.4Pa
28643	0.0020m	62528.4Pa
80204	0.0015m	62555.9Pa

The sensitivity of critical pressure predictions to meshing levels within the FEA is reported in Table 6. This variation of critical pressure also plotted in Figure 15 with rubber data based on a combination of all three Treloar data sets to determine the third order Ogden strain-energy function parameters.
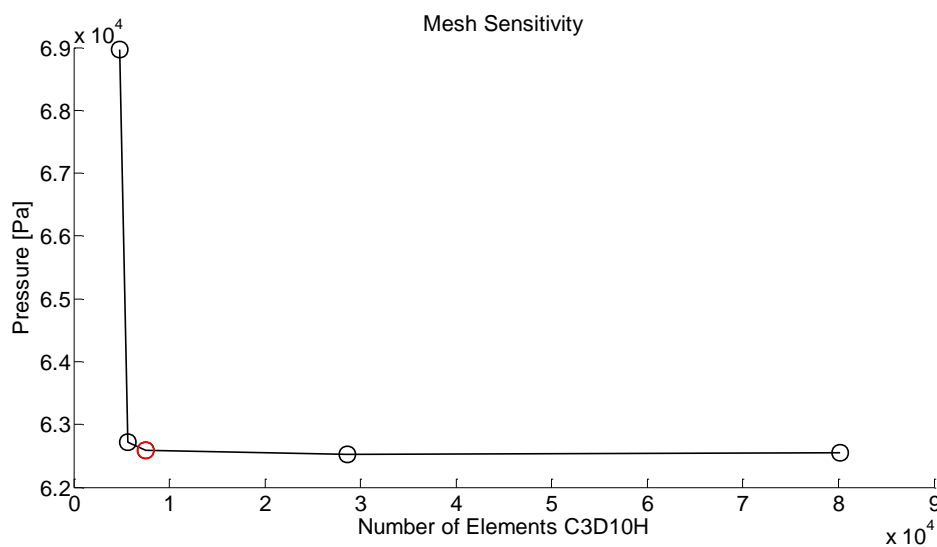
Fig. 15.   Mesh sensitivity

Figure 15 suggests that a correct order of magnitude of critical pressure is provided using 7553 elements.

Examination of the sensitivity of critical pressure to the strain-energy functions adopted is summarised in Table 7 for the cited discretization level. For the single distensible tube, Figure 7a indicates that the predicted critical pressure based on the third order Ogden model is the least sensitive to number of data set used. Other strain-energy functions are considerably more sensitive to the number and type of data sets used. Here, Table 7, based on using all the Treloar data reflects an expected wide variation of predicted critical pressure as a function of strain-energy function selected. It is not our intention to report influence of data sets combination for different strain-energy functions to provide an equivalent figure to Figure 7a. Given our observations concerning smaller variance of critical pressure prediction using third order Ogden, Figure 16 illustrates the change in geometry of a branched distensible tube once aneurysm development is commenced.

Table 7 Values of critical pressure for different strain-energy functions.

Strain-energy function	Critical pressure
Neo-Hookean	58736.9Pa
Yeoh	57008.4Pa
Arruda-Boyce	52206.0Pa
Mooney-Rivlin	65065.3Pa
Ogden N = 1	55243.9Pa
Ogden N = 2	64067.8Pa
Ogden N = 3	62585.4Pa
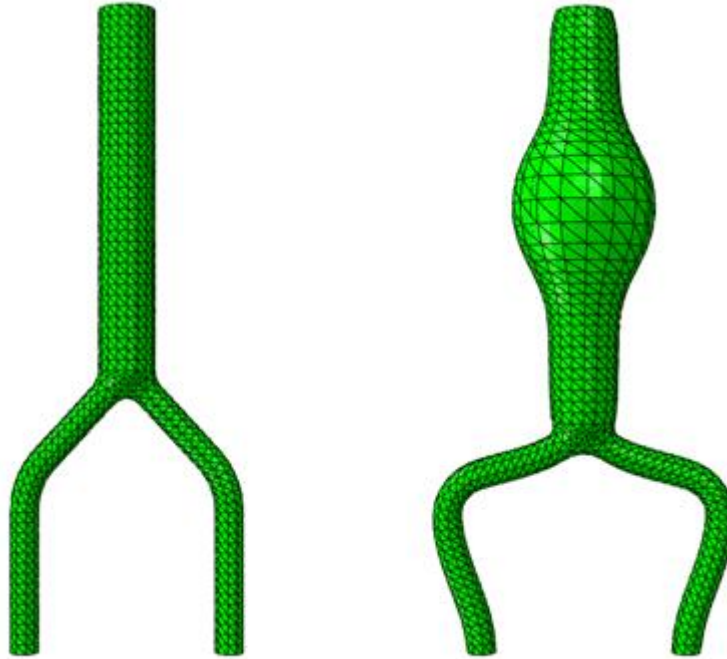
Fig. 16. Branched distensible tube with geometry analogous to abdominal aorta and iliac branches before and after aneurysm formation

Figure 16 differs from medical based aneurysm studies in so far as here the aneurysm has been developed from a branched distensible tube which was originally formed from purely cylindrical tubes. This is clearly different to artificially deforming the tube initially and then studying how pressure variation modifies the geometry. With due modesty, this analysis may be considered as a first attempt to formulate and solve the initiation of an aneurysm in a branched tube using FEA with a geometry comparable with an abdominal aorta and its iliac branches.

7. Conclusion and future work

The results presented allowed the making of the following observations:

- Consistency of finite element prediction is not affected by strain-energy function selected.
- The simple method is more useful as a solution starter for the membrane method.
- There is good consistency between the membrane method and the finite element method with membrane theory being slightly more consistent with the shell finite element analysis.
- Exploiting geometric symmetry does not adversely affect predicted results.
- The range of strain in Kawabata et al. data is smaller than that for the Treloar data, consequently the Kawabata stress-strain curves are simpler in geometric form and hence the

- fitting of strain-energy functions, irrespective of data selected, has significantly smaller variance.

- The larger range of strain in the Treloar data leads to points of the inflexion in the resulting stress-strain curves and it is this characteristic that appears to be responsible for the significantly larger variance of the critical pressure arising from combining different data sets to fit a selected strain-energy function.

- Engineering expectations would naturally select the maximum strain range possible for each form of data acquisition and having maximized the available data one might select strain-energy functions with a richer number of parameters to capture material behaviour.

- Equi-biaxial alone and uniaxial alone provide upper and lower boundaries of inflation pressure variation with the radial stretch parameter λ_1.

- Combined uniaxial, equi-biaxial and pure shear data provide inflation pressure variation with radial stretch parameter λ_1 that almost matched using a combination of uniaxial and equi-biaxial data.

- Use of the pure shear data alone is limited to the Neo-Hookean, Yeoh and Arruda-Boyce strain-energy functions dependent on I_1. Critical pressures of Neo-Hookean and Arruda-Boyce for Treloar and Kawabata are identical for each part of Tables B1 and B2.

- For the Kawabata et al. data Neo-Hookean and Arruda-Boyce strain-energy functions provide identical results irrespective of data sets used.

- For the more complex strain-energy functions dependent on both I_1 and I_2, pure shear data is not possible and for some data sets or combinations of data sets the data is deemed unstable. For these more complex functions critical pressure values tend to increase (in general, but not always) as the mathematical complexity of the function is increased.

- To verify, or otherwise, our conclusion in part A that higher Ogden and Yeoh models are preferable in the context of critical pressure and propagation pressure analysis, there is a real need to generate complete exhaustive testing of real rubber compounds to produce a greater choice of data sets. Whilst Kyriakides & Chang [15] provide Ogden parameters to their experimental data the rubber does not appear to be very different to the Treloar rubber. The raw experimental data is not provided and the μ_i and α_i fitted Ogden parameters $\left(kg/cm^2\right)$ are: 6.29, 0.019, –0.1 and 1.30, 5.08, –2.00 respectively, which are very similar to the Ogden fitting [11] of the original Treloar data provided in Equation (1) and column 3 of Table 1.

This research has concentrated on how critical pressure may be predicted, provided derivation of governing equations where deemed necessary, identified the consistencies of the alternative prediction methods and the variation of finite element applications for two readily available rubber data sets. Selection of t_{w0}/r_0 determines likelihood of aneurysm inception, not tube length, and hence single material tubes may require modification to prevent aneurysms, medically or engineering-wise. This is currently being investigated theoretically.

In this paper three distinct static approaches have been compared for the first time to demonstrate how they are related in terms of critical pressure predictions. This means we have clarified aspects about numerical simulation and provided guidelines about selection of strain-energy functions, their calibrations, selection of theoretical approach and elements for finite element formulations. All these aspects are of primarily concern for researchers in engineering fields where the aneurysm development assumes an important role. Furthermore, the scaling effect is explored for the first time and it has been demonstrated how all the different choices in the modelling steps can heavily affect the results of the simulation and its match with experimental data. The researcher can take advantages of these alternative approaches to produce different level of prediction accuracy according to time and resources available for the associated numerical analyses.

All the analyses within this paper and many of the cited references are based on static analysis. Detailed modelling in most cases will require a complete fluid-structure interaction model to give better insight. Such fluid structure interaction analyses are extremely time-consuming and situation dependent, especially when incompressible materials and fluids are involved. Here it is sufficient to say that the static analysis is a very necessary initial analysis to insure that new ideas and design have reason to be subject to the implied more complex dynamic analysis.

For engineering purposes the single distensible tube has relevance, whereas the branched distensible tube has relevance to both engineering and medical research.

Appendix A

This appendix provides strain-energy function parameters estimates for different combinations of uniaxial (U), equi-biaxial (E) and pure shear (P) for Treloar and Kawabata et al. materials. It will be observed that the Mooney-Rivlin and Ogden strain-energy functions have no parameter derivations based on use of pure shear data alone. For pure shear $\lambda_3 = 1$, $\lambda_1 = \lambda$ and so $\lambda_2 = 1/\lambda$. Hence $I_1 = I_2$ and the dependence of these strain-energy functions upon I_1 and I_2 cannot be captured using pure shear data. In other cases parameter values are omitted due to software detected instability during the fitting process. This ABAQUS$^®$ software state of instability is diagnosed using a test finite element to investigate behaviour of stress with changing strain [26]. When very large stress increases occur for very small strain increments numerical instability is declared.

Table A1   Mooney–Rivlin parameters

Treloar data (Appendix A of [1])			Kawabata et al. data [3]	
C_{10} [Pa]	C_{01} [Pa]	Data sets	C_{10} [Pa]	C_{01} [Pa]
210587.307	1504.76719	U/E/P	165640.263	4283.64967
225654.810	723.077386	U/E	168199.752	4002.21852
Unstable		U/P	151205.212	18659.3698
171395.981	4484.88823	E/P	171187.089	3258.40312
Unstable		U	132399.391	69720.4796
188677.067	3336.49811	E	206808.190	−1639.89324

Table A2   Ogden parameters

	Treloar data (Appendix A of [1])			Kawabata et al. data [3]	
N	μ [Pa]	α	Data sets	μ [Pa]	α
1	$\mu_1 = 359237.938$	$\alpha_1 = 2.11120130$	U/E/P	$\mu_1 = 396198.165$	$\alpha_1 = 1.65607343$
2	$\mu_1 = 42073.4586$	$\alpha_1 = 3.60405498$	U/E/P	$\mu_1 = 360506.823$	$\alpha_1 = 1.69468344$
	$\mu_2 = 360636.118$	$\alpha_2 = -0.03270528$		$\mu_2 = 32067.6210$	$\alpha_2 = -1.16772196$
3	$\mu_1 = 398206.801$	$\alpha_1 = 1.13176086$	U/E/P	$\mu_1 = 371516.221$	$\alpha_1 = 1.45516761$
	$\mu_2 = 5377.71517$	$\alpha_2 = 4.73211925$		$\mu_2 = 7642.20260$	$\alpha_2 = 3.98590415$
	$\mu_3 = 7647.41545$	$\alpha_3 = -2.14619240$		$\mu_3 = 15126.4287$	$\alpha_3 = -1.62520533$

1	$\mu_1 = 351146.363$	$\alpha_1 = 2.18594351$	U/E	$\mu_1 = 396960.176$	$\alpha_1 = 1.67730181$
2	$\mu_1 = 50935.0027$	$\alpha_1 = 3.49453801$	U/E	$\mu_1 = 313856.488$	$\alpha_1 = 1.85486372$
	$\mu_2 = 341658.313$	$\alpha_2 = -0.08026203$		$\mu_2 = 76794.6149$	$\alpha_2 = -0.56981938$
3	$\mu_1 = 397104.353$	$\alpha_1 = 1.16713591$	U/E	$\mu_1 = 365848.437$	$\alpha_1 = 1.51122161$
	$\mu_2 = 3475.35302$	$\alpha_2 = 4.97913398$		$\mu_2 = 3085.44716$	$\alpha_2 = 4.85887601$
	$\mu_3 = 7685.76954$	$\alpha_3 = -2.16788790$		$\mu_3 = 24242.5426$	$\alpha_3 = -1.33309384$
1	$\mu_1 = 312445.091$	$\alpha_1 = 2.22398921$	U/P	$\mu_1 = 389885.113$	$\alpha_1 = 1.64600146$
2	Unstable		U/P	$\mu_1 = 7134.83485$	$\alpha_1 = 4.07772362$
				$\mu_2 = 385806.221$	$\alpha_2 = 1.43803039$
3	$\mu_1 = 68511.5465$	$\alpha_1 = 3.12460724$	U/P	$\mu_1 = 389404.031$	$\alpha_1 = 1.44987755$
	$\mu_2 = 0.07034262$	$\alpha_2 = 10.3384903$		$\mu_2 = 3791.64258$	$\alpha_2 = 4.68810661$
	$\mu_3 = 342108.701$	$\alpha_3 = 0.02241924$		$\mu_3 = -0.10926884$	$\alpha_3 = -12.2916732$
1	$\mu_1 = 415943.662$	$\alpha_1 = 1.87886044$	E/P	$\mu_1 = 401039.902$	$\alpha_1 = 1.67510981$
2	$\mu_1 = 416910.689$	$\alpha_1 = 1.73012318$	E/P	$\mu_1 = 377603.874$	$\alpha_1 = 1.62206426$
	$\mu_2 = 727.119636$	$\alpha_2 = -3.06563173$		$\mu_2 = 18258.0747$	$\alpha_2 = -1.54908746$
3	$\mu_1 = 415000.046$	$\alpha_1 = 1.30510587$	E/P	$\mu_1 = 372203.856$	$\alpha_1 = 1.47327487$
	$\mu_2 = 3237.62981$	$\alpha_2 = 4.98702130$		$\mu_2 = 7648.68250$	$\alpha_2 = 3.69167649$
	$\mu_3 = 3192.12249$	$\alpha_3 = -2.47905674$		$\mu_3 = 15998.1343$	$\alpha_3 = -1.62642942$
1	$\mu_1 = 263263.880$	$\alpha_1 = 2.41450103$	U	$\mu_1 = 384747.397$	$\alpha_1 = 1.66804487$
2	$\mu_1 = 794.174092$	$\alpha_1 = 5.73957674$	U	$\mu_1 = 137.317773$	$\alpha_1 = 7.25441873$
	$\mu_2 = 367442.306$	$\alpha_2 = 1.53404686$		$\mu_2 = 388286.692$	$\alpha_2 = 1.55758121$
3	$\mu_1 = 93246.9186$	$\alpha_1 = 2.91596359$	U	Unstable	
	$\mu_2 = 0.11550173$	$\alpha_2 = 10.1311383$			
	$\mu_3 = 308210.545$	$\alpha_3 = -0.23814740$			
1	$\mu_1 = 427052.184$	$\alpha_1 = 2.08748534$	E	$\mu_1 = 406487.857$	$\alpha_1 = 1.90701322$
2	$\mu_1 = 433437.288$	$\alpha_1 = 1.70547134$	E	$\mu_1 = 374794.147$	$\alpha_1 = 1.39728754$
	$\mu_2 = 338.366920$	$\alpha_2 = -3.34932555$		$\mu_2 = 18488.5573$	$\alpha_2 = -1.76217330$
3	Unstable		E	Unstable	

Table A3   Neo–Hookean parameters

Treloar data (Appendix A of [1])	Data sets	Kawabata et al. data [3]
C_{10} [Pa]		C_{10} [Pa]
191999.034	U/E/P	183028.478
197482.041	U/E	185198.822
182901.819	U/P	176775.086
197537.128	E/P	188291.952
185263.958	U	174489.162
219910.806	E	201056.504
179383.516	P	179188.915

Table A4   Yeoh parameters

Treloar data (Appendix A of [1])			Data sets	Kawabata et al. data [3]		
C_{10} [Pa]	C_{20} [Pa]	C_{30} [Pa]		C_{10} [Pa]	C_{20} [Pa]	C_{30} [Pa]
190592.559	–1634.89996	41.3399927	U/E/P	197187.709	–4488.25309	177.629075
188258.146	–1386.21156	37.8669378	U/E	196726.363	–4053.13634	166.901802
179902.428	–1661.85611	42.2411003	U/P	193713.186	–4702.74588	172.404185
211077.700	–2974.55327	74.7048652	E/P	201084.695	–3912.25117	146.177404
167636.559	–1376.96240	39.9150124	U	190793.456	–5198.87204	219.299572
222164.258	–1892.78629	48.9352453	E	203941.679	–453.675959	3.12876288
201377.664	–3668.20550	99.9279490	P	197033.799	–4298.88146	133.444512

Table A5   Arruda–Boyce parameters

Treloar data (Appendix A of [1])		Data sets	Kawabata et al. data [3]	
μ [Pa]	λ_m		μ [Pa]	λ_m
332366.997	5.37292266	U/E/P	366056.948	6420.20926
332902.114	5.30761544	U/E	370397.638	7151.01182
306892.917	5.10704686	U/P	353550.168	8340.26732
383191.292	9.25324894	E/P	376583.898	7606.61247
288547.627	4.89038912	U	348978.321	9090.78585
415842.174	7.35966897	E	402113.005	8874.20437
358767.024	8904.31621	P	358377.827	9626.90878

Appendix B

Tables B1 provide critical pressure for different analyses using alternative Treloar data set combinations and various strain-energy functions. Tables B2 provide corresponding results for Kawabata et al. data.

Table B1 (a) Numerical results for critical pressure (Pa) using simple theory and Treloar data

| Model | Uniaxial | Uniaxial | Uniaxial | | Uniaxial | | |
| | Equi-biaxial | Equi-biaxial | | Equi-biaxial | | Equi-biaxial | |
	Pure shear		Pure Shear	Pure shear			Pure shear
Neo-Hookean	28794.5	29616.8	27430.1	29625.0	27784.4	32980.5	26902.5
Yeoh	28060.1	27787.9	26450.0	30726.3	24701.7	32712.8	29078.9
Arruda-Boyce	25681.4	25742.6	23792.3	29018.6	22440.8	31675.1	26902.5
Mooney-Rivlin	31961.0	34024.3	unstable	26839.8	unstable	29139.3	not possible
Ogden N=1	27060.6	26544.8	23665.7	31061.5	20177.5	32135.8	not possible
Ogden N=2	31567.7	31098.1	unstable	31125.3	27330.6	32277.7	not possible
Ogden N=3	30857.8	30589.6	32211.9	31441.5	32233.4	unstable	not possible

Table B1 (b) Numerical results for critical pressure (Pa) using membrane theory and Treloar data

| Model | Uniaxial | Uniaxial | Uniaxial | | Uniaxial | | |
| | Equi-biaxial | Equi-biaxial | | Equi-biaxial | | Equi-biaxial | |
	Pure shear		Pure Shear	Pure shear			Pure shear
Neo-Hookean	32508.4	33436.7	30968.1	33446.1	31368.0	37234.3	30372.4
Yeoh	31491.1	31214.1	29670.5	34357.1	27731.6	36714.6	32430.7
Arruda-Boyce	29072.1	29143.5	26942.6	32789.7	25420.1	35810.9	30372.4
Mooney-Rivlin	36018.0	38380.9	unstable	30102.3	unstable	32750.0	not possible
Ogden N=1	30890.0	30518.6	27305.9	34643.8	23612.3	36598.6	not possible
Ogden N=2	32104.3	31742.7	unstable	34190.7	29559.3	35381.9	not possible
Ogden N=3	32355.3	32090.2	33010.0	33386.6	33083.4	unstable	not possible

Table B1 (c) Numerical results for critical pressure (Pa) using FEM with shell element (S4R) and Treloar data

| Model | Uniaxial | Uniaxial | Uniaxial | | Uniaxial | | |
| | Equi-biaxial | Equi-biaxial | | Equi-biaxial | | Equi-biaxial | |
	Pure shear		Pure Shear	Pure shear			Pure shear
Neo-Hookean	32870.4	33721.8	31171.0	33730.1	31686.3	37668.5	30207.1
Yeoh	31275.9	30970.5	29980.7	34634.4	28013.6	36826.1	32121.8
Arruda-Boyce	29106.7	29164.4	27256.7	33131.3	25676.1	36162.2	30207.1
Mooney-Rivlin	36397.2	38752.9	unstable	30411.8	unstable	33022.3	not possible
Ogden N=1	31065.0	30469.0	27693.2	34722.6	24123.8	37046.1	not possible
Ogden N=2	32260.0	31920.1	unstable	34278.0	29465.4	35554.2	not possible
Ogden N=3	32487.7	32247.8	33188.5	33608.8	33286.3	unstable	not possible
Marlow	not possible	not possible	not possible	not possible	27291.5	34628.4	30185.6

Table B1 (d) Numerical results for critical pressure (Pa) using FEM with solid element (C3D20H) and Treloar data

Model	Uniaxial Equi-biaxial Pure shear	Uniaxial Equi-biaxial	Uniaxial Pure Shear	Equi-biaxial Pure shear	Uniaxial	Equi-biaxial	Pure shear
Neo-Hookean	32671.8	33606.5	31216.0	33617.0	31611.0	37513.4	30469.8
Yeoh	31700.2	31421.2	29864.6	34389.7	27527.1	36671.3	32615.1
Arruda-Boyce	29295.4	29339.4	27032.6	32919.5	25515.4	36060.2	30469.8
Mooney-Rivlin	36290.5	38679.6	unstable	30100.9	unstable	32309.0	not possible
Ogden N=1	30975.7	30718.0	27436.6	34761.8	23961.0	36942.0	not possible
Ogden N=2	32125.0	31753.3	unstable	34248.5	29645.5	35404.2	not possible
Ogden N=3	31964.8	31105.6	33019.1	32970.7	33104.9	unstable	not possible
Marlow	not possible	not possible	not possible	not possible	25566.9	34601.7	30064.3

Table B1 (e) Numerical results for critical pressure (Pa) using FEM with axisymmetric element (CAX8H) and Treloar data

Model	Uniaxial Equi-biaxial Pure shear	Uniaxial Equi-biaxial	Uniaxial Pure Shear	Equi-biaxial Pure shear	Uniaxial	Equi-biaxial	Pure shear
Neo-Hookean	32674.9	33602.9	31216.1	33613.4	31612.0	37515.4	30473.3
Yeoh	31699.6	31420.2	29865.4	34393.6	27531.6	36634.0	32614.7
Arruda-Boyce	29298.0	29363.7	27027.3	32918.3	25518.6	36053.7	30473.3
Mooney-Rivlin	36287.9	38521.3	unstable	30104.7	unstable	32314.7	not possible
Ogden N=1	30980.0	30722.0	27433.1	34751.2	23951.7	36940.4	not possible
Ogden N=2	32125.8	31754.4	unstable	34239.0	29644.0	35390.6	not possible
Ogden N=3	31942.1	31043.0	33020.3	32937.9	33103.8	unstable	not possible
Marlow	not possible	not possible	not possible	not possible	27156.2	34601.5	30063.8

Table B1 (f) Numerical results for critical pressure (Pa) using FEM with shell element (S4R) with clamped-symmetry boundary condition and Treloar data

Model	Uniaxial Equi-biaxial Pure shear	Uniaxial Equi-biaxial	Uniaxial Pure Shear	Equi-biaxial Pure shear	Uniaxial	Equi-biaxial	Pure shear
Neo-Hookean	32869.3	33720.2	31184.6	33728.5	31691.0	37668.4	30205.8
Yeoh	31334.5	30969.1	29980.6	34632.8	28012.7	36850.9	32197.8
Arruda-Boyce	29105.4	29163.2	27255.6	33129.9	25675.0	36168.8	30205.8
Mooney-Rivlin	36401.0	38751.3	unstable	30415.5	unstable	33020.7	not possible
Ogden N=1	31083.4	30507.5	27696.0	34720.7	24126.6	37049.0	not possible
Ogden N=2	32262.8	31921.7	unstable	34275.8	29463.3	35567.5	not possible
Ogden N=3	32485.4	32245.7	33190.8	33474.1	33285.6	unstable	not possible
Marlow	not possible	not possible	not possible	not possible	27297.8	34626.0	30186.0

Table B2 (a) Numerical results for critical pressure (Pa) using simple theory and Kawabata et al. data

Model	Uniaxial Equi-biaxial Pure shear	Uniaxial Equi-biaxial	Uniaxial Pure Shear	Equi-biaxial Pure shear	Uniaxial	Equi-biaxial	Pure shear
Neo-Hookean	27449.1	27774.6	26511.3	28238.5	26168.5	30152.8	26873.3
Yeoh	28248.6	28299.8	27666.3	28983.1	27112.0	30431.1	28261.6
Arruda-Boyce	27449.1	27774.6	26511.3	28238.5	26168.5	30152.8	26873.3
Mooney-Rivlin	25925.6	26237.3	27489.2	26496.9	38484.8	30603.6	not possible
Ogden N=1	29417.5	29487.7	28942.7	29789.3	28574.7	30382.3	not possible
Ogden N=2	29878.5	30083.5	29237.1	29914.8	28804.2	29648.0	not possible
Ogden N=3	29805.3	29824.2	29227.8	29916.9	unstable	unstable	not possible

Table B2 (b) Numerical results for critical pressure (Pa) using membrane theory and Kawabata et al. data

Model	Uniaxial Equi-biaxial Pure shear	Uniaxial Equi-biaxial	Uniaxial Pure Shear	Equi-biaxial Pure shear	Uniaxial	Equi-biaxial	Pure shear
Neo-Hookean	30989.5	31357.0	29930.7	31880.7	29543.7	34042.0	30339.4
Yeoh	31432.5	31533.3	30754.5	32311.8	30092.9	34298.6	31453.2
Arruda-Boyce	30989.5	31357.0	29930.7	31880.7	29543.7	34042.0	30339.4
Mooney-Rivlin	29079.2	29443.6	30147.6	29770.3	no max.	34621.4	not possible
Ogden N=1	32102.8	32244.3	31554.1	32567.3	31218.4	33982.1	not possible
Ogden N=2	32204.9	32335.3	31512.8	32222.6	31173.5	31309.9	not possible
Ogden N=3	31930.5	31911.7	31482.2	32039.1	unstable	unstable	not possible

Table B2 (c) Numerical results for critical pressure (Pa) using FEM with shell element (S4R) and Kawabata et al. data

Model	Uniaxial Equi-biaxial Pure shear	Uniaxial Equi-biaxial	Uniaxial Pure Shear	Equi-biaxial Pure shear	Uniaxial	Equi-biaxial	Pure shear
Neo-Hookean	31201.2	31673.2	29852.0	32250.6	29536.2	34253.0	30180.8
Yeoh	31700.5	31795.7	30774.7	31986.8	30354.4	34496.8	31720.6
Arruda-Boyce	31201.2	31673.2	29852.0	32250.6	29536.2	34253.0	30180.8
Mooney-Rivlin	29146.0	29583.3	30489.5	29920.8	no max.	34798.6	not possible
Ogden N=1	32365.1	32506.5	31817.0	32813.0	31465.8	34161.5	not possible
Ogden N=2	32347.0	32472.3	31754.4	32389.6	31411.9	31501.8	not possible
Ogden N=3	32096.9	32062.9	31723.3	32201.0	unstable	unstable	not possible
Marlow	not possible	not possible	not possible	not possible	29001.3	34758.5	31410.5

Table B2 (d) Numerical results for critical pressure (Pa) using FEM with solid element (C3D20H) and Kawabata et al. data

| Model | Uniaxial | Uniaxial | Uniaxial | | Uniaxial | | |
| | Equi-biaxial | Equi-biaxial | | Equi-biaxial | | Equi-biaxial | |
	Pure shear		Pure Shear	Pure shear			Pure shear
Neo-Hookean	31237.5	31600.3	30082.6	32098.7	29734.2	33429.1	30441.3
Yeoh	31529.4	31646.9	30910.8	32491.8	30176.2	33663.0	31549.9
Arruda-Boyce	31237.5	31600.3	30082.6	32098.7	29734.2	33429.0	30441.2
Mooney-Rivlin	29211.2	29544.1	30360.1	29851.9	no max.	34125.5	not possible
Ogden N=1	32177.5	32312.3	31663.8	32607.5	31347.8	33466.3	not possible
Ogden N=2	31160.2	32285.6	31581.4	32104.9	31279.6	31037.4	not possible
Ogden N=3	31631.5	30763.3	31552.8	31967.6	unstable	unstable	not possible
Marlow	not possible	not possible	not possible	not possible	29298.1	34565.7	31318.0

Table B2 (e) Numerical results for critical pressure (Pa) using FEM with axisymmetric element (CAX8H) and Kawabata et al. data

| Model | Uniaxial | Uniaxial | Uniaxial | | Uniaxial | | |
| | Equi-biaxial | Equi-biaxial | | Equi-biaxial | | Equi-biaxial | |
	Pure shear		Pure Shear	Pure shear			Pure shear
Neo-Hookean	31237.7	31601.2	30085.6	32100.7	29736.5	33435.2	30444.7
Yeoh	31533.9	31644.3	30911.8	32491.0	30167.6	33669.4	31552.8
Arruda-Boyce	31237.7	31601.2	30085.6	32100.7	28988.7	33435.2	30444.7
Mooney-Rivlin	29213.9	29547.2	30359.8	29855.2	no max.	34108.0	not possible
Ogden N=1	32179.7	32314.7	31665.3	32607.2	31348.9	33415.9	not possible
Ogden N=2	31101.2	32276.8	31582.9	32102.6	31280.7	31039.9	not possible
Ogden N=3	31835.0	30730.2	31554.5	31958.9	unstable	unstable	not possible
Marlow	not possible	not possible	not possible	not possible	29299.2	34131.1	31318.8

Table B2 (f) Numerical results for critical pressure (Pa) using FEM with shell element (S4R) with clamped-symmetry boundary condition and Kawabata et al. data

| Model | Uniaxial | Uniaxial | Uniaxial | | Uniaxial | | |
| | Equi-biaxial | Equi-biaxial | | Equi-biaxial | | Equi-biaxial | |
	Pure shear		Pure Shear	Pure shear			Pure shear
Neo-Hookean	31214.1	31678.1	29850.7	32251.1	29534.9	34251.5	30179.5
Yeoh	31699.5	31797.8	31036.9	31985.2	30353.6	34495.2	31719.6
Arruda-Boyce	31214.1	31678.1	29850.7	32251.1	29534.9	34251.5	30179.5
Mooney-Rivlin	29166.6	29599.1	30489.7	29936.5	no max.	34797.1	not possible
Ogden N=1	32364.0	32505.2	31817.5	32811.4	31468.6	34159.7	not possible
Ogden N=2	32344.8	32481.4	31753.6	32387.5	31413.7	31500.3	not possible
Ogden N=3	32094.8	32060.7	31722.6	32198.9	unstable	unstable	not possible
Marlow	not possible	not possible	not possible	not possible	29061.2	34757.8	31416.6

References

[1] A. Bucchi, G.E. Hearn, Predictions of Aneurysm Formation in Distensible Tubes – Part A – Theoretical Background to Alternative Approaches, International Journal of Mechanical Sciences, 71 (2013) 1–20.

[2] L.R.G. Treloar, Stress–strain data for vulcanised rubber under various types of deformation, Transactions of the Faraday Society, 40 (1944) 59–70.

[3] S. Kawabata, M. Matsuda, K. Tei, H. Kawai, Experimental Survey of the Strain Energy Density Function of Isoprene Rubber Vulcanizate, Macromolecules, 14 (1981) 154–162.

[4] J. Shi, G.F. Moita, The post-critical analysis of axisymmetric hyper-elastic membranes by the finite element method, Computer Methods in Applied Mechanics and Engineering, 135 (1996) 265–281.

[5] J.F. Rodriguez, C. Ruiz, M. Doblaré, G.A. Holzapfel, Mechanical Stresses in Abdominal Aortic Aneurysms: Influence of Diameter, Asymmetry, and Material Anisotropy, Journal of Biomechanical Engineering, 130 (2008) 021023–1 – 021023–10.

[6] D. Tang, C. Yang, D.N. Ku, A 3-D thin-wall model with fluid-structure interactions for blood flow in carotid arteries with symmetric and asymmetric stenoses, Computers and Structures, 72 (1999) 357–377.

[7] M.L. Raghavan, D.A. Vorp, Toward a biomechanical tool to evaluate rupture potential of abdominal aortic aneurysm: identification of a finite strain constitutive model and evaluation of its applicability, Journal of Biomechanics, 33 (2000) 475–482.

[8] J.R. Chaplin, V. Heller, F.J.M. Farley, G.E. Hearn, R.C.T. Rainey, Laboratory testing the Anaconda, Philosophical Transaction of the Royal Society of London. Series A, 370 (2012) 403–404.

[9] D. Pamplona, P.B. Goncalves, S.R.X. Lopes, Finite deformations of cylindrical membrane under internal pressure, International Journal of Mechanical Sciences, 48 (2006) 683–696.

[10] P.B. Goncalves, D. Pamplona, S.R.X. Lopes, Finite deformations of an initially stressed cylindrical shell under internal pressure, International Journal of Mechanical Sciences, 50 (2008) 92–103.

[11] R.W. Ogden, Large deformation isotropic elasticity – on the correlation of theory and experiment for incompressible rubber-like solids, Proceedings of the Royal Society of London, 326 (1972) 565–584.

[12] A. Needleman, Inflation of spherical rubber balloons, International Journal of Solids and Structures, 13 (1977) 409–421.

[13] D.M. Haughton, Post-bifurcation of Perfect and Imperfect Spherical Elastic Membranes, International Journal of Solids and Structures, 16 (1980) 1123–1133.

[14] E. Chater, J.W. Hutchinson, On the propagation of bulges and buckles, Journal of Applied Mechanics, 51 (1984) 269–277.

[15] S. Kyriakides, Y.C. Chang, On the inflation of a long elastic tube in the presence of axial load, International Journal of Solids and Structures, 26 (1990) 975–991.

[16] S. Kyriakides, Y.C. Chang, The initiation and propagation of a localized instability in an inflated elastic tube, International Journal of Solids and Structures, 27 (1991) 1085–1111.

[17] X. Guo, Kinematic modeling of finite axisymmetric inflation for an arbitrary polymeric membrane of revolution, Polymer-Plastics Technology and Engineering, 40 (3) (2001) 341–361.

[18] X. Guo, Large deformation analysis for a cylindrical hyperelastic membrane of rubber-like material under internal pressure, Rubber Chemistry and Technology, 74 (2001) 100–115.

[19] M. Kohandel, S. Sivaloganathan, G. Tenti, J.M. Drake, The constitutive properties of the brain parenchyma Part 1. Strain energy approach, Medical Engineering & Physics, 28 (2006) 449–454.

[20] Z. Gao, K. Lister, J.P. Desai, Constitutive Modeling of Liver Tissue: Experiment and Theory, Annals of Biomedical Engineering, 38 (2010) 505–530.

[21] B.J. Doyle, T.J. Corbett, A. Callanan, M.T. Walsh, D.A. Vorp, T.M. McGloughlin, An Experimental and Numerical Comparison of the Rupture Locations of an Abdominal Aortic Aneurysm, Journal of Endovascular Therapy, 16 (2009) 322–335.

[22] K.J. Bathe, Finite Element Procedures, Prentice Hall, Upper Saddle River (N.J.), 1996.

[23] E. Riks, An Incremental Approach to the Solution of Snapping and Buckling Problems, International Journal of Solids and Structures, 15 (1979) 529–551.

[24] J. Black, G. Hastings, Handbook of Biomaterial Properties, Chapman & Hall, London, 1998

[25] M. Street, Personal communication providing geometrical model for branched tube analysis, EDMC, Faculty of Engineering and the Environment, University of Southampton (2012).

[26] D. Cadge, A. Prior, Finite Element Modelling of Three-Dimensional Elastomeric Components, in: D. Boast, V.A. Coveney (Eds.), Finite Element Analysis of Elastomers, Professional Engineering Publishing, Bury St Edmunds, 1999, pp. 187–205.